



Eco-friendly screen-printed sensor using tapioca-based conductive ink modified with coconut fibers

Rafaela C. de Freitas^a, Jéssica Rocha Camargo^{a,*}, Laís Canniatti Brazaca^b, Lucio Angnes^c, Orlando Fatibello-Filho^d, Bruno C. Janegitz^{a,**}

^a Laboratório de Sensores, Nanomedicina e Materiais Nanoestruturados, Federal University of São Carlos, Araras, SP, Brazil

^b São Carlos Institute of Chemistry, University of São Paulo, São Carlos, SP, 13566-590, Brazil

^c Departamento de Química Fundamental, Instituto de Química, Universidade de São Paulo, Av. Prof. Lineu Prestes, 748 – 05508-000, São Paulo, SP, Brazil

^d Laboratório de Analítica, Bioanalítica, Sensores, Electroanalítica e Sensores, Departamento de Química, Universidade Federal de São Carlos (UFSCar), CP 676, 13560-970, São Carlos, SP, Brazil

ARTICLE INFO

Handling Editor: Prof Agata Michalska

Keywords:

Water-based conductive ink
Tapioca
Uric acid
Coconut fiber
Hydrogen peroxide

ABSTRACT

This study presents a novel eco-friendly water-based conductive ink composed of cassava starch (from tapioca flour) and sorbitol, combined with graphite powder and carbon black, for the fabrication of screen-printed electrodes. The electrochemical detection of uric acid was performed via differential pulse voltammetry, achieving a linear range of 5.0–100 $\mu\text{mol L}^{-1}$ and a detection limit of 0.34 $\mu\text{mol L}^{-1}$. The disposable sensors exhibited recovery rates ranging from 86.9 % to 112.1 % for synthetic urine and human serum samples. Additionally, a sensor was developed using the same conductive ink, incorporating coconut fiber into the formulation. Cyclic voltammetry was employed to detect hydrogen peroxide, with a linear range from 2.3 to 11.4 mmol L^{-1} and a detection limit of 0.6 $\mu\text{mol L}^{-1}$. The sensor demonstrated satisfactory performance for pharmaceutical applications, with recovery rates ranging from 90.3 % to 106.9 %. This work highlights the potential of water-based conductive inks using starch as a binder and coconut fiber in the development of sustainable electrochemical sensors, paving the way for environmentally friendly devices in analytical applications.

1. Introduction

In recent years there has been an increasing demand for the production of more sustainable materials to reduce waste generation and environmental pollution [1,2]. Discussions about the environment and sustainability have led to the establishment of the Sustainable Development Goals [1]. In this context, the development of biodegradable and less polluting products is becoming essential, along with aligning these products with the principles of circularity, encompassing production, consumption, restoration, and recycling [1,2].

Screen-printed electrochemical sensors have garnered significant interest due to their advantages, including relatively low cost, ease of use and production, minimal sample volume requirements for analysis, and potential for miniaturization. These characteristics make them portable and suitable for large-scale production [3,4]. Conductive inks play a critical role in the manufacturing process of these devices, particularly when using screen-printing techniques. These inks are

typically composed of conductive particles, binders, and/or additives, forming composites with conductive properties [5,6]. Also, the development of new water-based inks has emerged as a sustainable and environmentally friendly alternative, eliminating the need for organic solvents [6].

Along the same lines, biopolymers of plant origin have been highlighted for their use in several areas of the industry due to their film-forming capabilities, ease of obtaining, and relatively low cost [7]. Many biopolymers, including starches, are biodegradable. Starches are thermoplastics with a high capacity for molecular reorganization, which aligns with sustainability principles [7,8]. Among the many sources of starch, cassava stands out as a root from which starch can be extracted in the form of flour [7–9]. Tapioca flour (TP), derived from cassava, is a water-soluble, biodegradable polysaccharide composed of amylose and amylopectin linked through glycosidic bonds [8–10]. Films produced from tapioca exhibit properties such as good flexibility, low water permeability, and electrical non-conductivity, making tapioca an

* Corresponding author.

** Corresponding author.

E-mail addresses: jessica.10.camargo@gmail.com (J.R. Camargo), brunocj@ufscar.br (B.C. Janegitz).

<https://doi.org/10.1016/j.talanta.2025.128875>

Received 14 July 2025; Received in revised form 11 September 2025; Accepted 17 September 2025

Available online 18 September 2025

0039-9140/© 2025 Elsevier B.V. All rights are reserved, including those for text and data mining, AI training, and similar technologies.

excellent candidate as a binder for use in inks [7].

In the realm of environmentally friendly devices, sensors are particularly noteworthy. First-generation sensors, which rely on modifications with various enzymes, can be sustainably developed using components derived from *Cocos nucifera* L. (coconut) [11]. Coconut palms, originally from India, have been spread by oceanic currents throughout the tropical regions of the world, and their fruits yield numerous products and by-products, including water, milk, oil, charcoal, and coconut fiber [12,13]. Considering this, coconut fiber can be compared to carbon fiber, which has been utilized in electrochemical sensors to detect various compounds, including hydrogen peroxide (H_2O_2) [14,15]. Studies in the literature highlight the use of carbon fiber, as Wang et al. [15] developed a sensor for hydrogen peroxide by a platinum nanoparticle-modified carbon fiber microelectrode, demonstrating the potential of incorporating coconut fiber into conductive ink formulations to produce electrochemical sensors.

Some biomarkers have been detected by using screen-printed electrodes. Uric acid is the final product of purine metabolism in the human body and is found in various biological fluids [16]. Uric acid acts as an antioxidant, with normal levels in healthy individuals ranging from 26.0 to 72.0 mg/L [16,17]. As an important biomarker, uric acid is associated with several diseases, including type 2 diabetes, gout, hyperuricemia, arthritis, and conditions affecting the liver, neurological system, cardiovascular system, and kidneys [16]. Electrochemical methods are often employed for its determination, as demonstrated in the work of Turkkan et al. [18], who developed an electrochemical sensor by modifying a screen-printed electrode with Co_3O_4 nanoparticles and reduced graphene oxide for the detection of uric acid in synthetic saliva samples.

On the other hand, sensors can be utilized for detecting various molecules, including H_2O_2 . H_2O_2 is a small chemical compound commonly found in nature and is of interest across various industries, including pharmaceutical, clinical, environmental, textile, paper, and food [19,20]. Also, it plays a crucial role in the biological medium [20]. Quantifying H_2O_2 is also vital in industrial contexts, where it is used as a bactericide and bleaching agent [19]. An example of its electrochemical determination can be found in the study by Bilgi Kamac et al. [21], where a screen-printed electrode modified with reduced graphene oxide, poly (neutral red), and gold nanoparticles was developed for H_2O_2 detection.

In this work, a novel water-based conductive ink was developed using tapioca and sorbitol along with a mixture of graphite powder and carbon black for the fabrication of disposable screen-printed electrodes. These devices were applied to the determination of uric acid in biological fluid samples. Additionally, a sensor for hydrogen peroxide detection was manufactured using a conductive ink containing coconut fibers.

2. Experimental

2.1. Chemicals

All reagents of analytical grade used throughout this study were purchased from Sigma-Aldrich, Fisher, Dinâmica, Synth, and/or Fluka. Solutions were prepared using ultrapure Milli-Q water (resistivity $\geq 18.2 \text{ M}\Omega$) obtained from the Millipore™ Synergy® system. Electrochemical analyses were performed using AutoLab PGSTAT101 and 204 potentiostats/galvanostats, controlled by Nova 2.1.4 software. The electrochemical measurements utilized a three-electrode screen-printed system (comprising a working electrode, graphite/carbon black pseudo-reference electrode, and auxiliary electrode) fabricated with the developed conductive ink.

2.2. Morphological, structural, thermal, and electrochemical characterizations

The morphological characterizations were conducted using scanning

electron microscopy (SEM) with a Prisma E microscope (Thermo Fisher Scientific) operating in high vacuum at 10 kV, equipped with an Everhart-Thornley SE detector. Structural characterizations were performed using Fourier transform infrared spectroscopy (FTIR) with a Tensor II spectrophotometer (Bruker) at a resolution of 4.0 cm^{-1} and a scanning range of $400\text{--}4000 \text{ cm}^{-1}$ ($n = 64$). KBr pellets in a 1:100 ratio were prepared for the conductive ink, which consisted of graphite powder, carbon black, tapioca dispersion, tapioca flour, and sorbitol. Crystallographic analyses were performed using X-ray diffraction (XRD) with a Rigaku MiniFlex 600 X-ray powder diffractometer, employing a $\text{Cu K}\alpha$ radiation source ($\lambda = 0.15406 \text{ nm}$). Measurements were taken across an angular range of $2^\circ\text{--}90^\circ$, with a step size of 0.01° and a scanning speed of $10^\circ \text{ min}^{-1}$. Thermogravimetric analysis (TGA) was conducted in a nitrogen atmosphere with a flow rate of 20 mL min^{-1} . Temperature was varied from 30°C to 800°C at a heating rate of $10^\circ\text{C min}^{-1}$. Electrochemical characterizations were performed using cyclic voltammetry with 1.0 mmol L^{-1} potassium ferrocyanide/ferricyanide ($[\text{Fe}(\text{CN})_6]^{3-/4-}$) as the redox probe and 0.1 mol L^{-1} KCl as the supporting electrolyte.

2.3. Production of tapioca dispersion, the conductive ink and screen-printed electrodes

To produce the conductive ink, it was necessary to prepare a dispersion of tapioca flour in ultrapure water. The tapioca dispersion was prepared using 3 % (w/w) tapioca and 1 % (w/w) sorbitol as a plasticizer. To achieve the required gelatinization of the tapioca, the mixture was heated to 75°C under agitation for 30 min, following the method described by Mauruto et al. [11]. The conductive ink was prepared using graphite powder (35 % w/w, Fisher) and carbon black (10 % w/w, Cabot VXC72R) as conductive materials. A previously prepared water-based tapioca dispersion (3 % w/v tapioca and 1 % w/w sorbitol), served as the binder, as illustrated in Fig. 1A, step I. The ink was homogenized using a SpeedMixer (FlackTec Inc) at 1500 rpm for 90 s, repeated three times, step II. The screen-printed electrodes were fabricated using a screen with a 44-mesh pattern on an acetate substrate, step III. After printing, the electrodes were dried in an oven at 50°C for 48 h. They were then thermally treated at 90°C for 1 h. The three-electrode system's areas were delimited using a layer of nail polish as an insulating barrier, Step IV. The process can be watched in Video 1. It is worth mentioning that all optimization parameters for conductive ink were performed in a One-Variable-At-a-Time (OVAT) approach. Firstly, was varied the starch dispersion concentration, the concentration of conductive carbon materials, drying time, number of ink layers, and thermal treatment, in that order.

2.4. Preparation of uric acid and hydrogen peroxide samples

The synthetic urine used in this study was prepared as described by Campos et al. [22], consisting of 6.25 g of urea, 0.35 g of KH_2PO_4 , 0.73 g of NaCl, 0.56 g of Na_2SO_4 , 0.40 g of KCl, 0.27 g of $\text{CaCl}_2 \cdot 2\text{H}_2\text{O}$, and 25 g of NH_4Cl dissolved in 250 mL of PBS (pH 7.4). Uric acid samples were then prepared using the addition and recovery method within the same linear range as the analytical curve (section 2.7). Human serum, type AB (Sigma-Aldrich), was prepared as a 0.01 mol L^{-1} stock solution of uric acid. In this stock solution, uric acid samples were prepared via the addition and recovery method in 0.2 mol L^{-1} PBS (pH 7.4), maintaining the same linear range as the analytical curve. For hydrogen peroxide samples, a 20 % hydrogen peroxide solution (Beira Alta, São Paulo, Brazil) was purchased from a local cosmetics store. The analysis was conducted using the addition and recovery method in 0.2 mol L^{-1} PBS (pH 7.4), within the same concentration range as the analytical. Besides that, interferences were carried out for acid uric determination in the presence of $50 \mu\text{mol L}^{-1}$ in 0.2 mol L^{-1} PBS solution (pH = 7.0), containing dopamine, catechol, ascorbic acid, and urea in the same concentration (1:1).

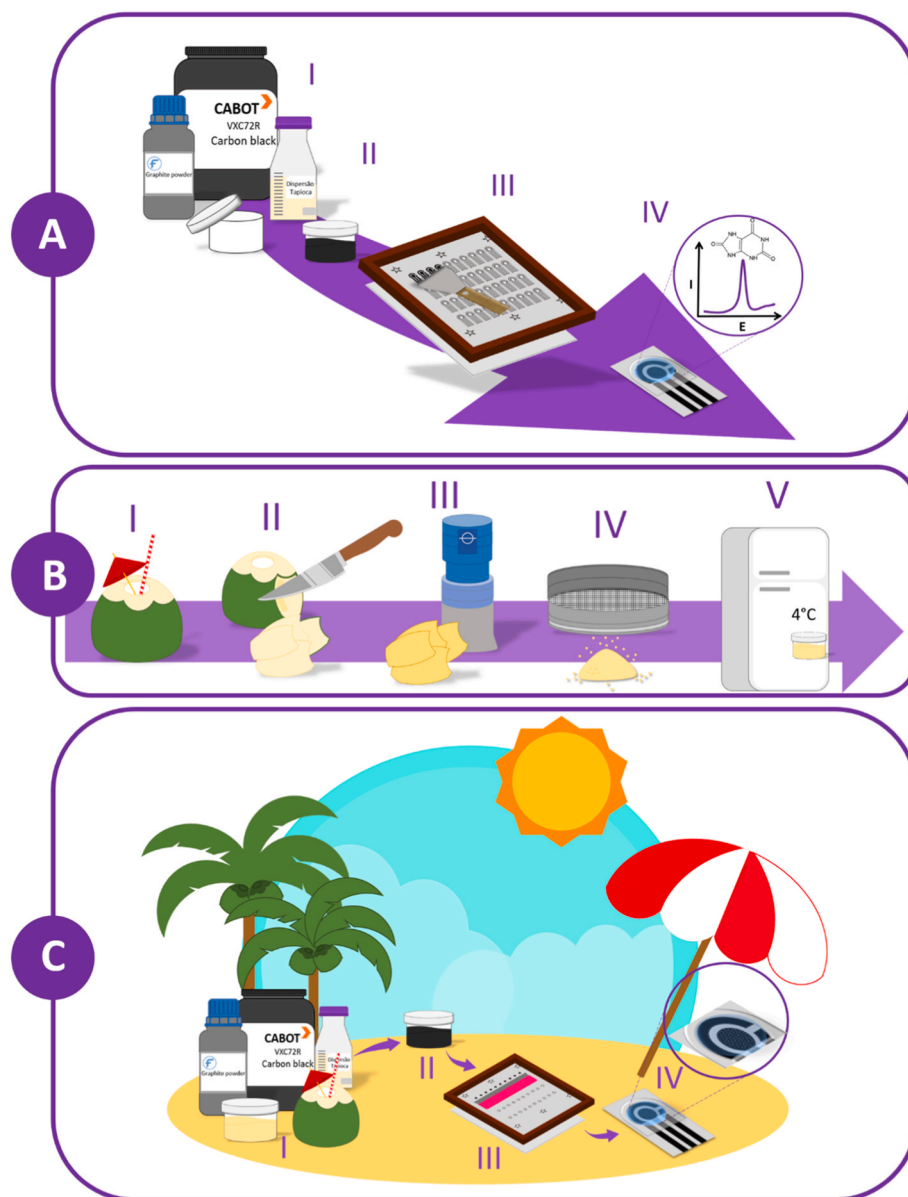


Fig. 1. (A) Manufacture of Conductive Ink and Screen-Printed Electrodes. (I) The components were weighed and prepared; (II) The conductive ink was mixed using the SpeedMixer; (III) The ink was spread over the surface of the screen, and the sensors were fabricated; (IV) Electrochemical measurements were performed after the sensors were dried and delimited. (B) Obtaining Coconut Fiber from Green Coconut. (I) Green coconut. (II) The white fibrous part of the coconut is extracted and cut into chips. (III) Coconut chips are dried and milled to reduce particle size. (IV) Sifting of coconut fibers to obtain a fine powder. (V) Coconut powder is stored in the refrigerator at 4 °C. (C) Fabrication process of the disposable screen-printed sensor. (I) Preparation of ink components, including conductive and binding materials; (II) Formulation of a conductive ink by incorporating coconut fiber (III) Deposition of the conductive ink onto the working electrode surface using a screen-printing technique, specifically targeting the working electrode area; (IV) Performance evaluation of the fabricated sensor through electrochemical measurements. (For interpretation of the references to color in this figure legend, the reader is referred to the Web version of this article).

2.5. Obtaining Coconut Fiber from green coconut

Coconut fibers were obtained following the method described by Kozan et al. [23]. The external part of the green coconut was removed to obtain the white fibrous part (step I), which was cut into chips (step II), and washed with acetonitrile. After this process, the fibers were dried in an oven at 30 °C until all solvents and moisture had completely evaporated. Next, the fibers were ground using a knife mill to reduce particle size (step III) and sifted to obtain a fine powder (step IV). Finally, the coconut powder was stored in a refrigerator at 4 °C (step V). The entire process is illustrated in Fig. 1B.

2.6. Production of the electrochemical sensor

The incorporation of coconut fibers into the ink formulation was achieved by adding them to the previously developed conductive ink, as shown in Fig. 1C. After preparing the ink, coconut powder was added to the composition in concentrations of 1 %, 5 %, and 10 % (w/w) relative to the weight of the tapioca dispersion. Once the coconut fibers were incorporated, the sensor was produced by using a screen to delimit only the working electrode. A layer of the modified conductive ink was then deposited onto the working electrode region of the screen-printed electrode. The device was subsequently dried for 12 h in a refrigerator, and the area of the three-electrode system was delimited using nail polish.

2.7. Uric acid and hydrogen peroxide determination

Uric acid detection was performed using electrochemical measurements based on pulse voltammetric techniques. Differential pulse voltammetry (DPV) and square wave voltammetry (SWV) were initially evaluated to determine the most suitable method. Given the data, DPV was selected for further analysis. To enhance analyte detection, chemical parameters were optimized, particularly pH, by testing different phosphate-buffered saline (PBS) solutions (0.2 mol L^{-1}) within a pH range of 5.0–8.0. Additionally, instrumental parameters such as pulse amplitude (a), step potential (s), and modulation time (t) were optimized. The optimal conditions were pH 7.0, $a = 80 \text{ mV}$, $s = 8.0 \text{ mV}$, and $t = 0.08 \text{ s}$. Under these conditions, an analytical calibration curve for uric acid was constructed over a concentration range of 5.0–100 $\mu\text{mol L}^{-1}$. Further validation was performed through analyses in synthetic urine and human serum samples.

Hydrogen peroxide detection was conducted using electrochemical assays based on cyclic voltammetry (CV) at a scan rate of 25 mV s^{-1} , within a potential range of 0.0–0.6 V. The resulting analytical curve demonstrated a linear response for hydrogen peroxide concentrations ranging from 2.3 to 11.4 mmol L^{-1} in PBS (0.2 mol L^{-1} , pH 7.4).

3. Results and discussion

3.1. Optimization and preparation of conductive ink

A 6 % (m/V) tapioca dispersion was prepared in ultrapure water to develop a new water-based conductive ink using tapioca. To ensure homogeneous dispersion, the effect of plasticizers was investigated, with the addition of 1 % (w/w) glycerin or sorbitol. This formulation allowed the addition of 40 % (w/w) graphite, which was applied to a screen-printed electrode (SPE). The finished device design is shown in Fig. S1. The conductivity of the ink was evaluated using cyclic voltammetry (CV) for $1.0 \text{ mmol L}^{-1} [\text{Fe}(\text{CN})_6]^{3-/4-}$ in $0.1 \text{ mol L}^{-1} \text{ KCl}$ at a scan rate of 50 mV s^{-1} . Fig. S2 presents the characteristic electrochemical peaks for inks formulated using both plasticizers. The dispersion containing glycerin exhibited an oxidation peak at 83 mV and a reduction peak at -34 mV , resulting in a ΔE_p of 117 mV and an anodic-to-cathodic current ratio (I_{pa}/I_{pc}) of 1.19. For the sorbitol-based dispersion, the oxidation and reduction peaks appeared at 76 mV and -27 mV , respectively, yielding a ΔE_p of 103 mV and an I_{pa}/I_{pc} ratio of 1.04. Based on these results, the tapioca-based conductive ink containing sorbitol demonstrated a lower ΔE_p and higher electrochemical reversibility when compared to the glycerin formulation. These results can be associated with the stronger interactions between starch-sorbitol [24]. Therefore, sorbitol was selected as the preferred plasticizer for ink formulation. Further studies were conducted to evaluate factors influencing conductivity, such as the number of ink layers (1 and layers) and drying time. These experiments were performed via CV for $1.0 \text{ mmol L}^{-1} [\text{Fe}(\text{CN})_6]^{3-/4-}$ and $0.1 \text{ mol L}^{-1} \text{ KCl}$ at 50 mV s^{-1} , with results in Figs. S3 and S4, respectively. For the drying study, the voltammograms presented a lightly capacitive and resistive profile, which was improved in the subsequent studies. The results indicated the enhancement in anodic and cathodic current magnitudes for electrodes printed with two layers of conductive ink and dried for 48 h.

To enhance the current magnitude, three different formulations were prepared by incorporating two carbon materials, graphite (GR) and carbon black (CB), while maintaining a fixed total carbon conductive material content of 45 % (w/w). The tested compositions included: 42.5 % GR/2.5 % CB, 40 % GR/5 % CB, and 35 % GR/10 % CB, all using a 6 % (w/V) tapioca dispersion with 1 % (w/w) sorbitol. Electrochemical characterizations were performed using CV in $1.0 \text{ mmol L}^{-1} [\text{Fe}(\text{CN})_6]^{3-/4-}$ and $0.1 \text{ mol L}^{-1} \text{ KCl}$ at 50 mV s^{-1} . As shown in Fig. S5A, all formulations exhibited characteristic electrochemical profiles. However, the 42.5 % GR/2.5 % CB composition demonstrated the poorest performance, with less-defined oxidation and reduction peaks and

overall irreversible behavior. In contrast, the 40 % GR/5 % CB and 35 % GR/10 % CB formulations exhibited similar quasi-reversible electrochemical profiles, with ΔE_p values of 502 mV and 500 mV, respectively, and I_{pa}/I_{pc} ratios of 0.97 and 0.99. To achieve a higher current response, the 35 % GR/10 % CB formulation was selected for further studies. Despite variations in carbon material proportions, capacitive current effects were significant in the electrochemical sensors. This behavior may be attributed to the polymeric network structure of tapioca, which influences charge transfer processes by affecting the double-layer charging at the electrode-solution interface [10]. As a result, the faradaic current from the redox process of the electroactive species was less pronounced. To address this issue, new ink formulations were prepared, containing lower amounts of tapioca (3 % and 4 % (w/V)), while maintaining 1 % (w/w) sorbitol and 35 % GR/10 % CB. Electrochemical analyses, performed via CV under the same conditions, are presented in Fig. S5B. Both formulations exhibited similar electrochemical behavior, with oxidation and reduction peaks appearing at approximately 0.1 V and -0.2 V , respectively, yielding ΔE_p values of around 300 mV and I_{pa}/I_{pc} ratios of approximately 0.93. The reduction in tapioca concentration resulted in more defined electrochemical profiles and lower peak potential variations, classifying both formulations as quasi-reversible. Finally, the 35 % GR/10 % CB formulation in a 3 % (w/V) tapioca dispersion with 1 % (w/w) sorbitol was selected as the final composition for the electrochemical sensor preparation.

3.2. Electrochemical characterization of the Gr-CB-S-TP/acetate

The SPE fabricated using the 35 % GR/10 % CB conductive ink with a 3 % (w/V) tapioca dispersion and 1 % (w/w) sorbitol was designated Gr-CB-S-TP/acetate. Based on the drying study, the electrodes were subjected to thermal treatment in an oven at temperatures ranging from 50°C to 100°C for 1 h. The impact of this treatment was evaluated using cyclic voltammetry (CV) for $1.0 \text{ mmol L}^{-1} [\text{Fe}(\text{CN})_6]^{3-/4-}$ in $0.1 \text{ mol L}^{-1} \text{ KCl}$ solution at 50 mV s^{-1} , with results presented in Fig. S6. A significant change in the electrochemical profile was observed compared to untreated electrodes, with oxidation peaks around 0.03 V and reduction peaks near -0.07 V . However, no substantial shift in peak potential was observed across different temperatures. Thermal treatments at 80°C and 100°C produced higher oxidation current responses compared to the other conditions, but they also exhibited greater variability between replicates. The treatment at 90°C , although not yielding the highest current response, was selected for device application due to its better peak definition and lower standard deviation, ensuring complete water evaporation. At 100°C , higher deformation of the electrode substrate was observed, making this temperature unsuitable for further processing.

After defining the best thermal treatment ($=90^\circ\text{C}$), cyclic voltammetry (CV) was performed using the Gr-CB-TP/acetate sensor for $1.0 \text{ mmol L}^{-1} [\text{Fe}(\text{CN})_6]^{3-/4-}$ in $0.1 \text{ mol L}^{-1} \text{ KCl}$ at 50 mV s^{-1} . As shown in Fig. 2A, the electrochemical profile exhibited well-defined oxidation and reduction peaks at 110 mV and -130 mV , respectively, with a calculated ΔE_p of 240 mV. The anodic and cathodic peak currents were 124 mA and -128 mA , yielding an I_{pa}/I_{pc} ratio of 0.97. These results indicate that the system can be classified as quasi-reversible. This was considered based on the fact that the electrochemical system as a whole consists of three carbon electrodes, which are non-conventional and fabricated using a lab-made conductive ink.

To evaluate the electrochemical behavior of the sensor, CV measurements were conducted at scan rates ranging from 10 to 100 mV s^{-1} in $1.0 \text{ mmol L}^{-1} [\text{Fe}(\text{CN})_6]^{3-/4-}$ and $0.1 \text{ mol L}^{-1} \text{ KCl}$. The results, shown in Fig. 2B and C, were analyzed using oxidation and reduction peak currents following the Randles-Sevcik equation:

$$\Delta I_p = \pm 2.63 \times 10^5 \times A \times C \times D^{1/2} \times n^{3/2} \times \Delta \nu^{1/2}$$

where, I_p refers to the peak currents (A), A is electroactive area will to be

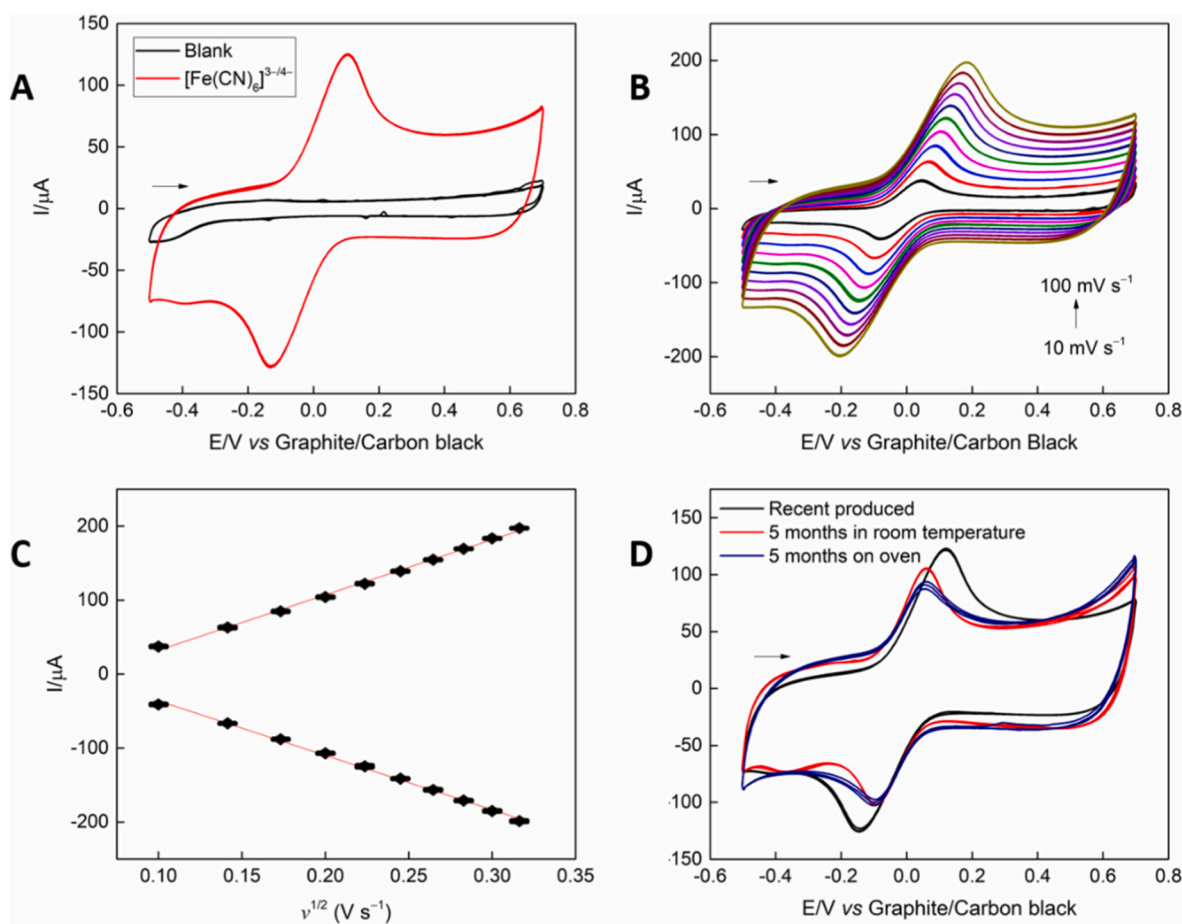


Fig. 2. (A) Cyclic voltammograms (CVs) of the Gr-CB-TP/acetate sensor recorded in the absence (black line) and presence (red line) of $1.0 \text{ mmol L}^{-1} [\text{Fe}(\text{CN})_6]^{3-/4-}$ and $0.1 \text{ mol L}^{-1} \text{ KCl}$ at a scan rate of 50 mV s^{-1} ; (B) Cyclic voltammograms of the Gr-CB-S-TP/acetate sensor recorded in $1.0 \text{ mmol L}^{-1} [\text{Fe}(\text{CN})_6]^{3-/4-}$ and $0.1 \text{ mol L}^{-1} \text{ KCl}$, with scan rates varying from 10 to 100 mV s^{-1} ; (C) Correlation between $v^{1/2}$ vs. peak current (I); (D) Stability study. Cyclic voltammograms obtained with ink-based printed sensors with Gr-CB-S-TP/acetate sensor in presence of $1.0 \text{ mmol L}^{-1} [\text{Fe}(\text{CN})_6]^{3-/4-}$ in $0.1 \text{ mol L}^{-1} \text{ KCl}$ solution, at 50 mV s^{-1} .

calculated (cm^2), C is a concentration (mol cm^3) and D is electrochemical probe diffusion coefficient ($7.8 \times 10^{-6} \text{ cm}^2 \text{ s}^{-1}$), n is electron number presents in reaction and v is the scan rate (V s^{-1}). Based on this analysis, the electroactive area of the device was estimated at 1.045 cm^2 , which is 7.5 times larger than its geometric area of 0.136 cm^2 . In the literature, other SPEs are also found where the electroactive area has been calculated. For example, Camargo et al. [25] reported a value of 0.69 cm^2 for a device made with a conductive ink based on graphite powder and nail polish. Similarly, Orzari et al. [26] obtained a value of 0.172 cm^2 for an SPE fabricated with a conductive ink containing only carbon black as the conductive material. Comparing these results, the electroactive area calculated in our study is higher than those reported by others. This difference may be attributed to the presence of two different conductive carbon materials in our electrode, which could enhance its electrochemical activity. In addition, at higher scan rates, the characteristic oxidation and reduction peaks of the electrochemical probe were still observed; however, they did not exhibit a proportional relationship between peak magnitude and increasing scan rates.

The stability study for the sensor was conducted to evaluate its useful lifespan for electrochemical detection applications. This was done by comparing the device's response after 5 months of storage at room temperature and in an oven at 50°C to that of a newly produced sensor. Fig. 2D shows the CV curves obtained in $1.0 \text{ mmol L}^{-1} [\text{Fe}(\text{CN})_6]^{3-/4-}$ in $0.1 \text{ mol L}^{-1} \text{ KCl}$ solution at 50 mV s^{-1} . It is observed that both devices exhibit a decrease in anodic and cathodic currents after 5 months of storage. The reduction is more pronounced in the oven-stored device, with a current decrease of approximately 1.3 times. Despite this

decrease, the results are considered acceptable, given the long storage period and the fact that the electrodes were stored without packaging or special conditioning.

To verify the stability of the carbon pseudo-reference, CV was carried out in the presence of $1.0 \text{ mmol L}^{-1} [\text{Fe}(\text{CN})_6]^{3-/4-}$ in $0.1 \text{ mol L}^{-1} \text{ KCl}$ solution at 50 mV s^{-1} , in 3 sensors and for 3 scans each. This study was made using the SPE with a carbon pseudo-reference and another with the reference electrode printed with a silver conductive ink, thus being a silver pseudo-reference. The voltammograms are shown in Fig. S7, where it is possible to observe a displacement of potential anodic and cathodic potential peaks of the electrochemical probe between the different reference electrodes. However, both of them showed stable and without variation of potential in your self-system, proving no necessity to print the reference electrode with silver conductive ink, and that the carbon can also be used as a pseudo-reference electrode in this case. Besides that, there are present in literature other disposable SPEs that use carbon conductive inks as pseudo-reference electrodes [27–29].

The electrochemical characterization was also performed using electrochemical impedance spectroscopy (EIS) to evaluate the interaction between the electrode surface and the solution. In Fig. S8, it is possible to observe the Nyquist diagrams obtained by EIS for the Gr-CB-TP/acetate sensor (A) and the CF-Gr-CB-TP/acetate sensor (B), over a frequency range from 1.0×10^5 to $1.0 \times 10^{-1} \text{ Hz}$. The measurements were taken with 10 points per decade, an amplitude of 10 mV , and sinusoidal waves, applying a potential of 0.05 V , which corresponds to the half-wave potential. Both devices exhibit similar behaviors, resulting in a system modeled by three parallel resistance (R) and constant phase

element (Q) components arrange in series, represented by the equivalent circuit [R (RQ) (RQ) (RQ)]. The behavior observed in the Nyquist plots indicates a significant capacitive influence, with lower resistance facilitating current flow. Also, the equivalent circuit represents the presence of three phases, which are likely related first to the most exposed material, probably graphite, as suggested by the SEM images, followed by carbon black, and finally the conductive composite as a whole. It is also possible to consider a series-layer model, since the electrode was manufactured by screen-printing with two layers of conductive ink [30]. This circuit additionally suggests that the electrode has a porous surface, a condition similar to the diffusional mass transfer model of a uniform transmission line. In this case, the solution fills the pores, so the resistance of the pore material can be considered negligible, and the only relevant resistance is the ohmic drop of the electrolyte. Consequently, the theoretical Nyquist plot exhibits a straight line at 45° at high frequencies, which may result from charge saturation at the pore ends, where the pores block any direct current from passing through the electrode substrate [31,32]. Since the conductive ink developed in this work is water-based, this property may also influence the pore filling. Additionally, the starch polymer used as a binder likely contributes to this interaction (see Fig. S9).

3.3. Morphological, structural, and thermal characterizations

The morphological characterization of the developed device was

analyzed using SEM at magnifications of $50\times$, $1000\times$, and $2000\times$, as shown in Fig. 5. The SEM images of the tapioca dispersion (Fig. 3A) reveal the formation of a film with visible cracks, likely resulting from the drying process. At higher magnifications, the surface appears smooth and homogeneous. The acetate substrate (Fig. 3B) exhibits a rough surface at all magnifications, which may enhance the ink adhesion during the printing process. The screen-printed electrode surfaces (Fig. 3C and D) show no significant differences between them. At $50\times$ magnification, the working electrode surface appears rough but demonstrates uniform ink deposition on the acetate substrate. However, in Figs. 3C–1, a higher presence of pores is noticeable. At $1000\times$ and $2000\times$ magnifications, graphite flakes are identifiable, along with spherical agglomerates, which can be attributed to carbon black.

Fig. 4A presents the FTIR spectra of the conductive ink, graphite (GR), carbon black (CB), tapioca polymer (TP), sorbitol, and the 3 % TP/1 % sorbitol dispersion. Due to the similarity in functional groups between tapioca and the plasticizer sorbitol, their spectra, as well as the spectra of their combined dispersion, exhibit similar vibrational bands. In the $2920\text{--}2895\text{ cm}^{-1}$ range, C–H symmetric and asymmetric stretching bands are observed [33]. Bands around 1015 cm^{-1} correspond to C–O–H stretching vibrations, while those at 1410 cm^{-1} are related to bending modes, which are more intense in sorbitol [33]. The spectra of tapioca dispersion and tapioca show C–O–C bands between 940 and 900 cm^{-1} , associated with glycosidic bonds in amylose [34]. For carbon materials (GR and CB), a peak at 1635 cm^{-1} corresponds to

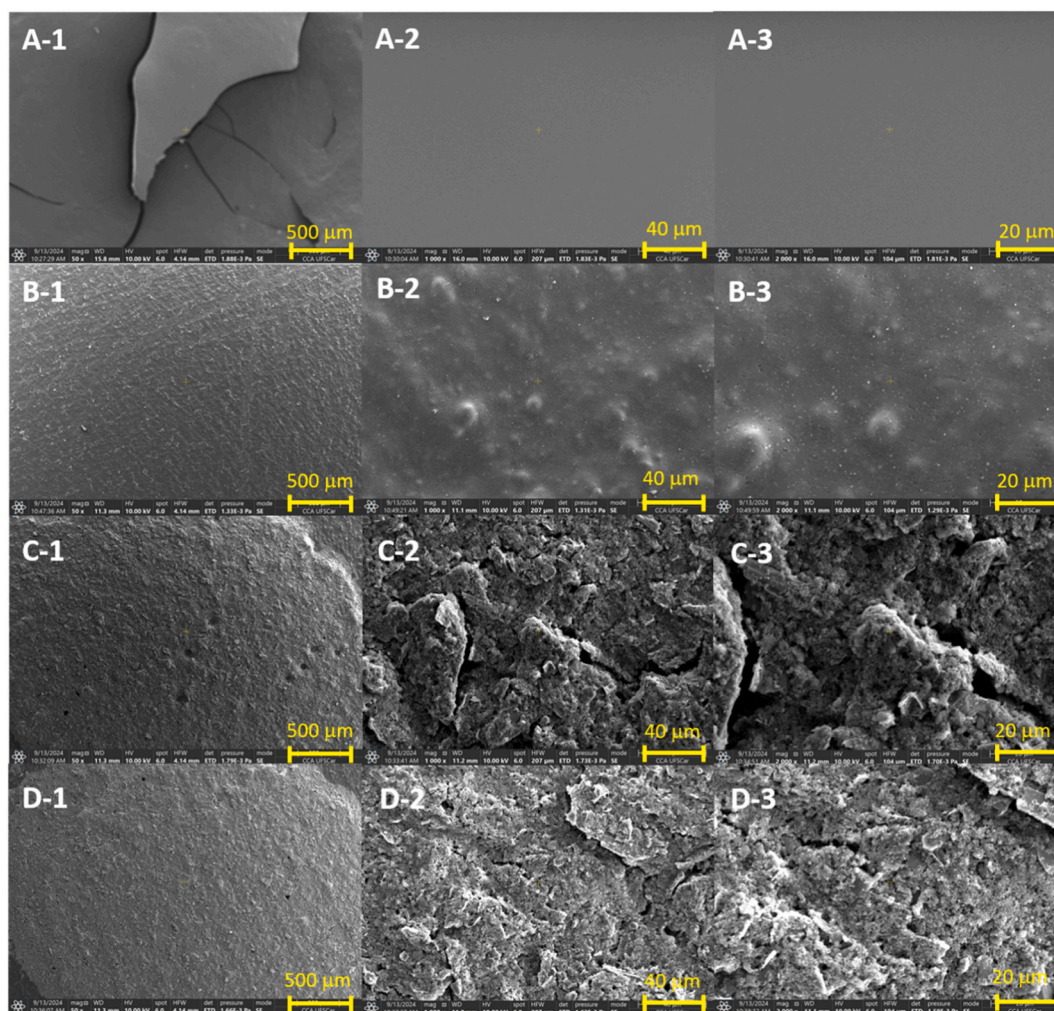


Fig. 3. SEM images of the samples: (A) tapioca dispersion, (B) acetate substrate, (C) electrode dried for 48 h, and (D) electrode thermally treated at 90°C . Images are shown at magnifications of $50\times$ (1), $1000\times$ (2), and $2000\times$ (3).

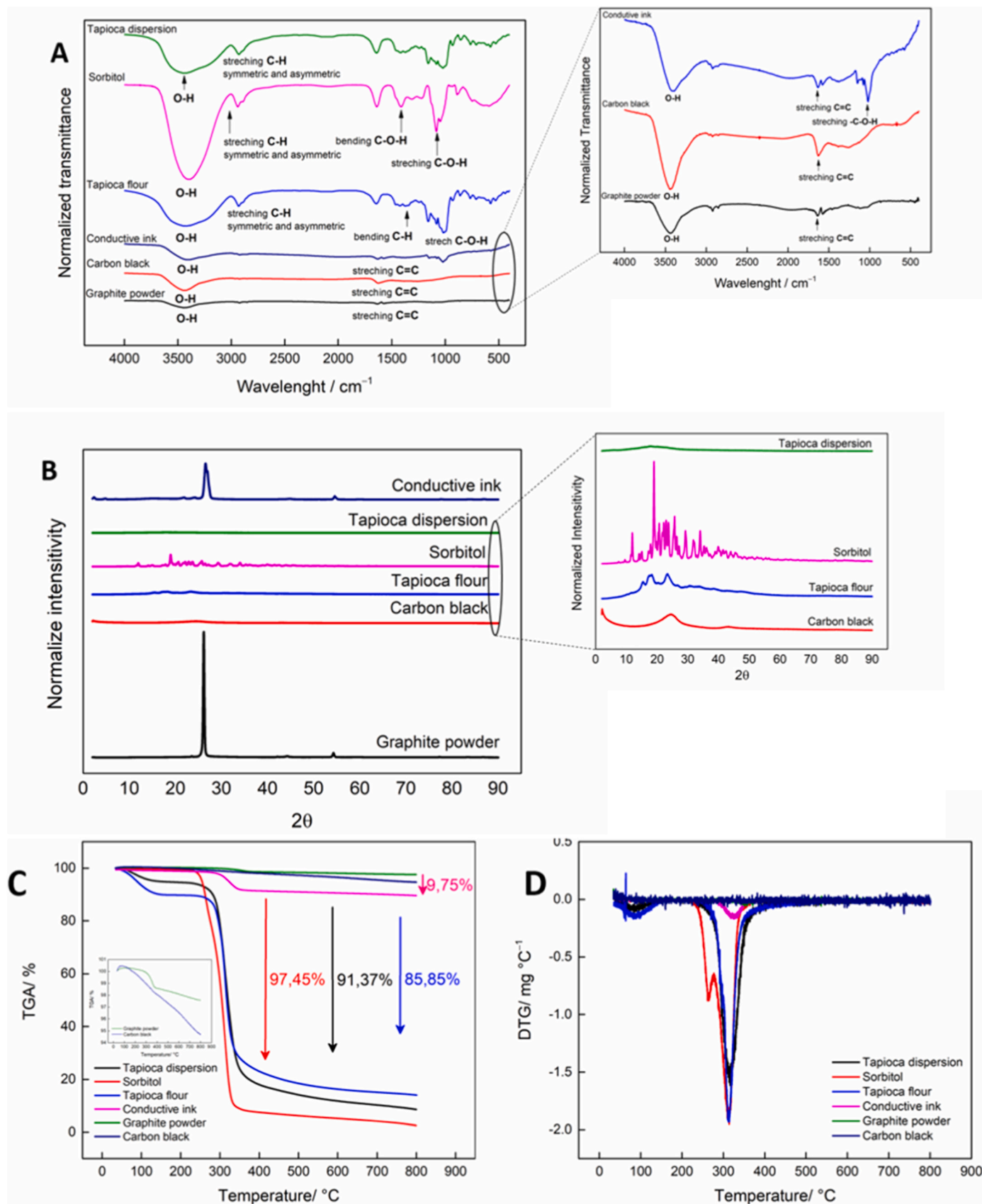


Fig. 4. (A) FTIR spectra of the samples: conductive ink (dark blue), tapioca dispersion (green), tapioca flour (blue), sorbitol (pink), carbon black (red), and graphite (black). (B) X-ray diffraction (XRD) patterns of the same samples. (C) Thermogravimetric analysis (TGA) curves for conductive ink (pink), tapioca dispersion (black), tapioca flour (blue), sorbitol (red), carbon black (dark blue), and graphite (green). (D) Differential thermogravimetric (DTG) curves of the corresponding samples. (For interpretation of the references to color in this figure legend, the reader is referred to the Web version of this article).

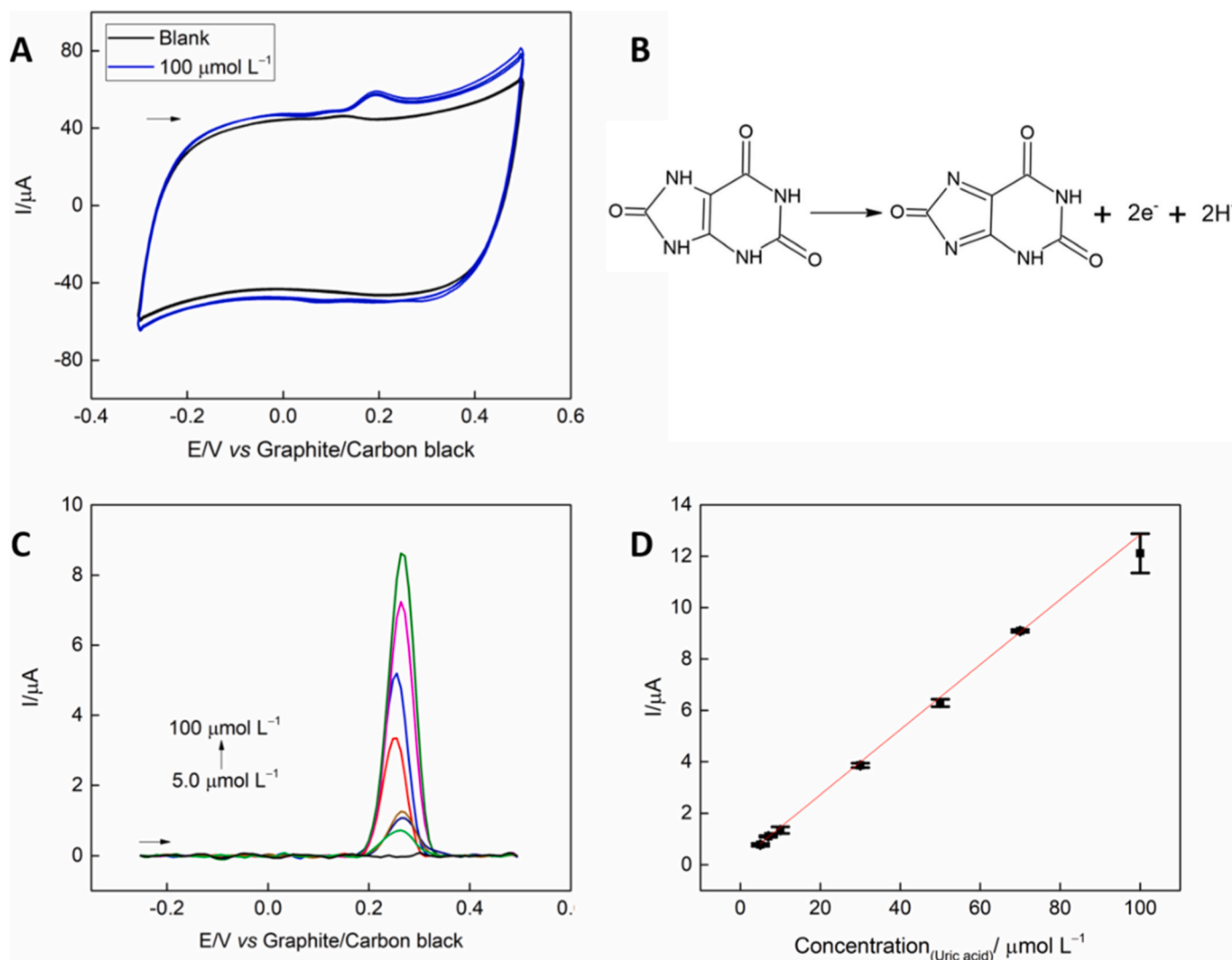


Fig. 5. (A) CVs obtained using the Gr-CB-S-TP/acetate sensor for $100 \mu\text{mol L}^{-1}$ uric acid in 0.2 mol L^{-1} PBS (pH 7.0), with a scan rate of 50 mV s^{-1} . (B) Proposed oxidation mechanism of uric acid. (C) DPV obtained with the Gr-CB-TP/acetate sensor for uric acid detection, with concentrations varying from 5.0 to $100 \mu\text{mol L}^{-1}$ in 0.2 mol L^{-1} PBS (pH 7.4) under optimized conditions: step potential = 8.0 mV , amplitude = 25 mV , and modulation time = 0.08 s . (D) Correlation between uric acid concentration and peak current response ($n = 3$, with different sensors).

$\text{C}=\text{C}$ stretching from sp^2 hybridization, as expected [33]. The FTIR spectrum of the conductive ink confirms the incorporation of all constituent materials. Characteristic peaks at 1635 cm^{-1} and 1020 cm^{-1} correspond to $\text{C}=\text{C}$ bonds in conductive materials and $\text{C}-\text{O}-\text{H}$ bonds from TP and sorbitol, respectively [33]. Additionally, strong bands around 3400 cm^{-1} indicate $\text{O}-\text{H}$ bond vibrations, with higher wavenumbers corresponding to free $\text{O}-\text{H}$ vibrations from humidity, and lower wavenumbers indicating hydrogen-bonded $\text{O}-\text{H}$ groups [33].

The XRD patterns shown in Fig. 4B were obtained for the same samples analyzed in FTIR. Tapioca dispersion and carbon black exhibit amorphous patterns, as expected for CB [35]. Sorbitol displays characteristic crystalline peaks at $2\theta = 11.9^\circ, 14.2^\circ, 15.0^\circ, 17.2^\circ, 17.8^\circ, 18.9^\circ, 20.6^\circ, 22.0^\circ, 22.9^\circ, 23.7^\circ, 25.7^\circ, 26.4^\circ, 27.2^\circ, 29.2^\circ, 31.8^\circ$, and 34.1° , corresponding to its γ -phase [36]. Tapioca flour presents peaks at $2\theta = 15.4^\circ$ and 23.3° , with broad peaks at 17.5° and 18.3° , characteristic of C-type crystallinity typical of root starches [37]. Graphite exhibits a sharp peak at $2\theta = 26.2^\circ$, corresponding to the (002) plane, with a calculated particle size of 28.39 nm [27]. The conductive ink exhibits a diffraction pattern similar to graphite, but with a slight peak shift at $2\theta = 26.5^\circ$, corresponding to a calculated particle size of 9.47 nm . This shift suggests interactions and agglomeration of ink components during

formulation, a phenomenon also observed in Orzari et al. [38].

Thermogravimetric analysis (TGA) was conducted to assess the thermal stability of the conductive composite. The TGA and DTG curves are presented in Figs. 4C and 6D. Tapioca polymer (TP), as the main binder, undergoes thermal degradation associated with $\text{C}-\text{C}$, $\text{C}-\text{H}$, and $\text{C}-\text{O}-\text{H}$ bond cleavage, as indicated by FTIR. It shows a residual mass of 14.15% at 800°C , with degradation occurring between 238 and 368°C , peaking at 312°C , consistent with literature values [39]. Sorbitol exhibits a higher degradation rate, with a residual mass of 2.55% . Its decomposition range (222 – 275°C) aligns with the breakdown of bonds also found in TP [40]. The 3% TP/1 % sorbitol dispersion degrades between 233 and 376°C , peaking at 314°C . It shows higher degradability than pure TP, with a residual mass of 8.63% , indicating improved thermal stability due to reduced water content [41]. The conductive ink exhibits the highest thermal stability, degrading between 270 and 370°C , leaving a residual mass of 90.25% . This high stability is likely due to the large proportion of GR and CB, which occurs once graphite degradation begins around 900°C [42].

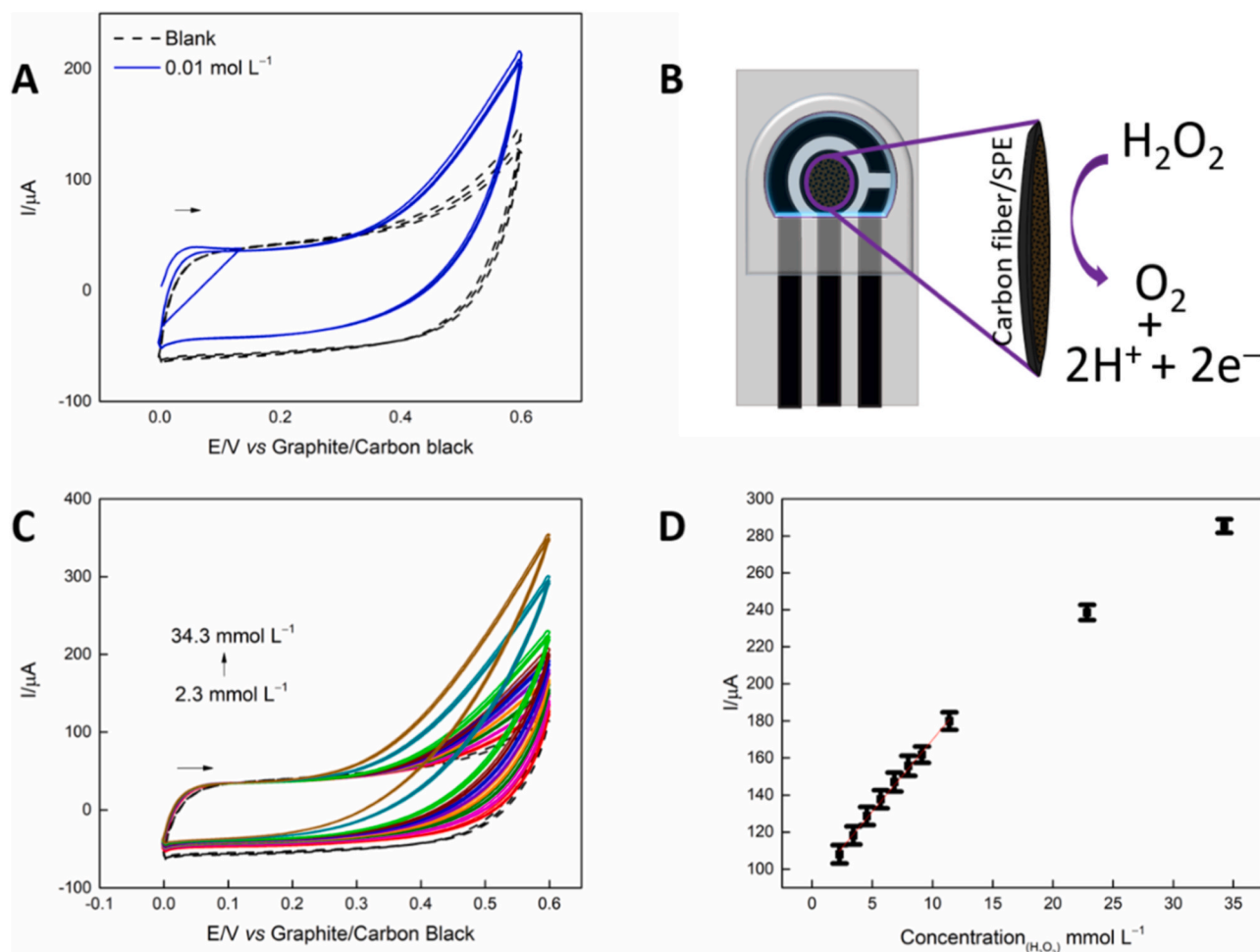


Fig. 6. (A) CVs were recorded using the CF-Gr-CB-S-TP/acetate sensor with 2 % CF in a 0.01 mol L⁻¹ H₂O₂ solution prepared in 0.2 mol L⁻¹ PBS (pH 7.4) at a scan rate of 25 mV s⁻¹. (B) Proposed oxidation mechanism of H₂O₂ reaction on the sensor surface. (C) Cyclic voltammograms obtained with CF-Gr-CB-S-TP/acetate sensor for H₂O₂, varying the concentration from 2.3 to 34.3 mmol L⁻¹ in 0.2 mol L⁻¹ PBS solution (pH = 7.4), ν = 25 mV s⁻¹. (D) Correlation concentration vs current (n = 3).

3.4. Electrochemical determination of uric acid and analytical curve

Uric acid is a significant biomarker, serving as a metabolic antioxidant in the human body. Fluctuations in its levels within biological fluids are associated with various diseases, including diabetes, arthritis, cardiovascular, neurological, and renal disorders. Therefore, its detection was investigated as a proof of concept for the SPE fabricated using the developed conductive ink. To assess the electrochemical behavior of uric acid, cyclic voltammetry (CV) was performed for 100 μmol L⁻¹ uric acid in 0.2 mol L⁻¹ phosphate-buffer medium (PBS, pH 7.0) at a scan rate of 50 mV s⁻¹. The results, shown in Fig. 5A, reveal an oxidation peak at approximately 0.2 V. These findings align with the work of Sakthivel et al. [43], which proposed an oxidation mechanism for uric acid occurring at the electrode surface, involving the deprotonation of two amine groups to form dehydrourate (Fig. 5 B).

Differential pulse voltammetry (DPV) and square wave voltammetry (SWV) were evaluated to optimize the device's performance for the detection of uric acid. Electrochemical analyses were conducted in a 100 μmol L⁻¹ uric acid solution prepared in 0.2 mol L⁻¹ PBS (pH 7.0) (Fig. S10). Both techniques exhibited an oxidation peak at approximately 0.2 V; however, DPV demonstrated better peak definition and a higher current response. Specifically, DPV produced a signal 4.43 times higher than SWV, making it the preferred method for further studies and analytical quantification. Subsequently, key chemical and instrumental parameters of DPV were optimized, including pH (ranging from 5.0 to

8.0 in 0.2 mol L⁻¹ PBS), amplitude (10–100 mV), step potential (1–10 mV), and modulation time (0.01–0.1 s), all for 100 μmol L⁻¹ uric acid. Based on the results, the optimal parameters were established as pH = 7.0, amplitude = 80 mV, step potential = 8.0 mV, and modulation time = 0.08 s.

Under optimized parameters, an analytical curve was constructed by varying uric acid concentrations from 5.0 to 100 μmol L⁻¹ in 0.2 mol L⁻¹ PBS (pH 7.0) (n = 3). As shown in Fig. 5C, the analytical curve exhibited good linearity within the studied range, yielding the linear equation: $I_p (A) = 0.1264 \times C_{(uric\ acid)} (mol\ L^{-1}) - 1.92 \times 10^{-7}$, and $r^2 = 0.999$, Fig. 5D. The limit of detection (LOD) was calculated using formula 3 × standard deviation of blank divided by slope, resulting in a value of 0.34 μmol L⁻¹. Reproducibility between similar electrodes was evaluated using 50 μmol L⁻¹ uric acid in 0.2 mol L⁻¹ PBS (pH 7.0), yielding a relative standard deviation (RSD) of 8.99 % (n = 4). However, repeatability studies were not performed, as the SPE exhibited a significant decrease in oxidation peak intensity after the first measurement. This decrease can be attributed to electrode surface poisoning, which does not significantly affect the usability of the SPE, which is a single-use disposable device.

4. Oxidation detection of hydrogen peroxide on a screen-printed sensor containing coconut fiber

4.1. Electrochemical determination of H_2O_2

Based on the work of Kozan and collaborators [23], CF was obtained from fresh green coconut. The first ink composition tested contained 5 % (w/w) CF powder. These inks exhibited a granular texture, with visible fiber incorporation. However, electrode printing was not uniform in this case, as the fibers obstructed the screen pores. The electrochemical device was dried overnight, and after delimiting the droplet area, CV was performed at 25 mV s^{-1} for $0.1 \text{ mol L}^{-1} H_2O_2$ in 0.2 mol L^{-1} PBS (pH 7.4). The addition of 5 % CF influenced the response, showing interference effects in the absence of H_2O_2 . With 10 % CF, the sensor displayed a resistive profile, indicating that increasing the coconut fiber content hindered electron transfer. To optimize the ink composition, new formulations were developed with CF concentrations ranging from 2 % to 4 % (w/w). The respective CVs are presented in Fig. S11. The best printing performance was achieved with 2 % CF, which prevented screen clogging.

Sensors manufactured with this optimized ink were analyzed via CV at 25 mV s^{-1} for $0.01 \text{ mol L}^{-1} H_2O_2$ in 0.2 mol L^{-1} PBS (pH 7.4), as shown in Fig. 6. In Fig. 6A, no distinct peak for the target analyte was observed; instead, oxygen evolution, resulting from H_2O_2 oxidation, was detected at more positive potentials as concentration increased [23], consistent with the mechanism illustrated in Fig. 6B, this involves the oxidation of H_2O_2 , resulting in the formation of oxygen gas through the transfer of two electrons and two protons, when this mechanism also was proposed for others sensors which used carbon fiber [44,45]. Besides that, the sensor developed by Seven et al. [46] based on nanoporous carbon fiber microelectrode presented electrocatalytic activity for H_2O_2 detection, with an electrochemical profile on oxidation similar to that obtained in this work, and correlating the lower anodic current with the slow kinetics of carbon electrodes. Also, the sensor with 2 % CF exhibited the most significant electrochemical response. Although a higher CF content could suggest the influence of electrocatalytic activity, the presence of other components, such as cellulose, likely impeded charge transfer and masked the other activities. Another possible explanation about the profile can be related with the probable presence of metals in trace levels on coconut fiber, as iron (Fe), zinc (Zn) and copper (Cu) [47,48], that already was related as compounds in different parts of coconut fruit. The presence of these metals can auxiliary on H_2O_2 detection, once many works on literature used metallic nanoparticles for this purpose in electrochemical sensors for this molecule [49,50]. An example, is the sensor developed by Liu et al. [50] that used Cu in an alloy with palladium (Pd) to improve the catalytic activity for H_2O_2 oxidation, and the alloy PdCu obtained a higher oxidation current compared with the electrode modified only with Pd. Consequently, subsequent H_2O_2 determination experiments were conducted using conductive ink containing 2 % (w/w) CF.

To confirm that the observed electrochemical behavior is attributed to the addition of CF on conductive ink, comparative electrochemical tests were conducted. The sensor fabricated with 2 % (w/w) CF in conductive ink was analyzed alongside a bare SPE coated with an additional layer of conductive ink without CF. Cyclic voltammetry (CV) was performed at a scan rate of 25 mV s^{-1} for $0.01 \text{ mol L}^{-1} H_2O_2$ in 0.2 mol L^{-1} PBS (pH 7.4). As shown in Fig. S12, the sensor containing 2 % (w/w) CF exhibited a more pronounced current response, indicating greater oxygen evolution compared to the SPE without CF. This difference can be attributed to the catalytic activity of CF as a source of carbon fibers.

The device was also evaluated for the determination of H_2O_2 using chronoamperometry. Measurements were performed in the absence and presence of 1.0 and 10 mmol L^{-1} in 0.2 mol L^{-1} PBS (pH 7.4), applying 0.5 V for 60 s, as shown in Fig. S13. The results demonstrate an increase in current with higher concentrations of H_2O_2 , indicating that this

technique is suitable for quantifying the compound.

After defining the CF composition, CV analyses were performed at a scan rate of 25 mV s^{-1} for H_2O_2 , with concentrations ranging from 2.3 to 34.3 mmol L^{-1} in 0.2 mol L^{-1} PBS (pH 7.4), to construct an analytical curve, as shown in Fig. 6C and D. A fixed potential of 0.55 V was applied to record anodic currents corresponding to oxygen evolution, revealing a linear response from 2.3 to 11.4 mmol L^{-1} . The resulting linear equation was $I_{pa} = (0.00776 \pm 1.85 \times 10^{-4}) \times C(H_2O_2) (\text{mol L}^{-1}) - 0.922 \times 10^{-5} \pm 1.32 \times 10^{-6}$, with a limit of detection (LOD) calculated as 0.6 mmol L^{-1} . The non-linearity observed at higher concentrations is associated with the saturation of the working electrode activity. To assess the repeatability and reproducibility of the device, CV measurements were performed at 25 mV s^{-1} for $5.7 \text{ mmol L}^{-1} H_2O_2$ in 0.2 mol L^{-1} PBS (pH 7.4). The obtained relative standard deviation (RSD) values were 3.54 % ($n = 3$) for repeatability and 1.53 % ($n = 3$) for reproducibility.

5. Electrochemical detection of uric acid in biological fluids and H_2O_2 in pharmaceutical samples

To evaluate the electrochemical device's performance for uric acid determination, analyses were conducted in synthetic urine and human serum using the standard addition and recovery method within the linear range of the analytical curve. The measurements were performed using the DPV technique with optimized parameters, as shown in Table 1. The recovery values ranged from 86.91 % to 109.3 % for synthetic samples and from 94.71 % to 112.1 % for human serum samples. Uric acid levels can vary depending on the type of biofluid. In blood, concentrations typically range from 26 to 75 mg/L , while in urine, secretion levels can reach up to 750 mg/L [16,51]. Therefore, these results demonstrate that the sensor offers satisfactory analytical performance for uric acid detection in clinical samples, considering the need for sample dilution. For the sensor evaluation, the electrochemical performance was assessed in pharmaceutical samples of oxygenated water (20 vol%) (H_2O_2) using cyclic voltammetry (CV) at a scan rate of 25 mV s^{-1} in 0.2 mol L^{-1} PBS (pH 7.4). The recovery values, obtained using the standard addition and recovery method, ranged from 90.33 % to 106.9 %, as presented in Table 1. These results demonstrate that the developed sensor provides satisfactory performance for H_2O_2 determination in pharmaceutical samples within the analytical range. Since the concentration of H_2O_2 in these products is relatively high, only simple dilution is required for sample preparation.

Considering potential interferences in the uric acid analysis, the influence of $50 \text{ } \mu\text{mol L}^{-1}$ of the analyte was studied in the presence of ascorbic acid, catechol, dopamine, and urea at the same concentration. Table S1 presents the impact of these interferents as percentages. For the compounds tested, a decrease in the uric acid current was observed, with

Table 1

Determination of uric acid in synthetic urine and human blood serum samples and H_2O_2 pharmaceutical samples.

Samples	Add ($\mu\text{mol L}^{-1}$)	Recovery ($\mu\text{mol L}^{-1}$)	Percentage (%)
Synthetic urine (uric acid -sensor)			
1	5.0	5.46 ± 0.09	109
2	7.0	6.08 ± 0.1	86.9
3	30	30.9 ± 0.5	103
4	50	46.4 ± 0.2	92.8
5	70	67.6 ± 0.8	96.5
6	100	95.9 ± 0.2	95.9
Human male blood serum Type AB (uric acid -sensor)			
1	7.0	6.7 ± 0.2	96.4
2	10	11.2 ± 0.2	112
3	50	48.3 ± 0.5	96.6
4	70	66.3 ± 0.2	94.7
Oxygenated water - 20 vol (Hydrogen peroxide- sensors)			
1	5.0	4.5 ± 0.1	90.3
2	5.0	5.34 ± 0.05	107

the most interference caused by ascorbic acid, which reduced the response by -15.6% . The compound that least interfered with uric acid detection was catechol, resulting in a current decrease of -7.82% . These results are expected, as the sensor does not have any modifications to make it highly selective for uric acid, allowing some level of interference from these substances. The same study was also performed for H_2O_2 detection in the same conditions as previously for uric acid detection. All the compounds showed influence in the determination of H_2O_2 , only ascorbic acid increased the response by 32.2% . Others result in the decrease of response of H_2O_2 in -16.6 , -30.9 and -8.24% for catechol, dopamine and urea. This indicates that if the sensor were applied to samples with these substances, it would influence the H_2O_2 determination; however, in the proposed and analyzed samples, these components are not present.

6. Comparison with other devices in the literature

The determination of uric acid in biological samples is of great clinical interest and the search for electrochemical sensors in the literature is growing in the last years. Kanyong et al. [52] modified a screen-printed electrode (SPE) with reduced graphene oxide and determined uric acid using differential pulse voltammetry (DPV). Their sensor exhibited a wide concentration range, and a lower limit of detection (LOD) compared to the other studies. Jirakunakorn et al. [53] and Cruz et al. [54] both developed sensors for uric acid using Prussian blue-modified SPEs and the uricase enzyme. However, the key difference between these studies lies in the additional modifications: the former incorporated graphene cryogel and chitosan, while the latter used poly (4-aminosalicylic acid). Both sensors demonstrated acceptable concentration ranges but had higher LODs than other reported devices. Fanjul-Bolado et al. [55] developed a sensor using a multi-walled carbon nanotube-modified SPE for uric acid detection. This device achieved a linear range comparable to that obtained in the present study. Based on the comparison of these collected studies, the fabricated disposable electrochemical device in this work exhibited a satisfactory linear detection range and LOD for uric acid. Moreover, it highlights the advantages of minimal electrode surface modification, making it a more cost-effective and sustainable alternative. Similarly, several electrochemical devices for H_2O_2 detection in various samples can be found in the literature. Maksuk et al. [56] developed a non-enzymatic amperometric sensor based on a porous gold-modified SPE, achieving a wide linear range for H_2O_2 oxidation and a low LOD. Other studies employed glassy carbon electrodes (GCE) for modification. For instance, Devaraj et al. [57] developed a sensor incorporating horseradish peroxidase in a chitosan-graphene oxide-gold nanocomposite, achieving a lower quantification range but a higher LOD for H_2O_2 reduction. Additionally, several studies utilized metallic nanoparticle modifications for H_2O_2 detection. Bian et al. [58] and Guler et al. [59], developed sensors incorporating platinum-polypyrrole microspheres and bimetallic nanoparticles functionalized with reduced graphene oxide, respectively. Given that the present study employed cyclic voltammetry (CV) for H_2O_2 detection, the developed sensor demonstrated an acceptable analytical response for the target analyte. Its linear range is comparable to those reported in the literature, with only one cited device achieving detection in the $\mu\text{mol L}^{-1}$ range. Table S2 compares collected studies that report analyte detection using electrochemical devices.

7. Greenness metric

In the search for reducing environmental impacts in diverse areas, models have been suggested in recent years to evaluate the green aspect of analytical methods used to determine different compounds. One of them is the AGREE – Analytical Greenness metric developed by Pena-Pereira et al. [60]. This scoring scale aims to classify greenness quantitatively, based on the 12 principles of green analytical chemistry. The scale ranges from 0.0 (red) to 1.0 (green), where the most presented

results of 1.0 indicate the most environmentally friendly analytical methods. The figure generated for this metric consists of a circle with twelve principles numbered from 1 to 12. The color of each number corresponds to the score obtained for that principle. Therefore, this metric was applied using the Pena-Pereira et al. [60] software to calculate the greenness of the present work, which yielded a score of 0.89, as shown on the scale in Fig. S14. This result is satisfactory on the scale, as it is also similar to other SPE devices in the literature. One of them is the work of Soliman et al. [61], which obtained a score of 0.76 for a system using a screen-printed potentiometric sensor for valproate. In the review by Habdías-Netos et al. [62], the AGREE scores for different ePADs were compared, and those obtained by screen-printing were in the range of 0.79–0.83.

8. Conclusion

This study demonstrated the feasibility of producing a sustainable and novel water-based conductive ink using TP as a binder and a combination of conductive materials (GR and CB) was demonstrated. A new conductive ink was successfully formulated with a composition of 35 % (w/w) GR, 10 % (w/w) CB, and a dispersion of 3 % (w/V) TP and 1 % (w/V) sorbitol. This ink was applied to fabricate screen-printed electrodes on an acetate substrate. Its use in the electrochemical determination of uric acid resulted in a linear range of $5.0\text{--}100\ \mu\text{mol L}^{-1}$, with a LOD of $0.34\ \mu\text{mol L}^{-1}$, enabling reliable recovery in fortified biological fluid samples with high reproducibility. Additionally, the conductive ink was modified with green coconut fiber to develop an electrochemical sensor for H_2O_2 detection. This sensor exhibited a linear detection range for hydrogen peroxide from 2.3 to $11.4\ \text{mmol L}^{-1}$, with a LOD of $0.6\ \text{mmol L}^{-1}$, demonstrating its applicability for pharmaceutical hydrogen peroxide analysis with high efficiency. The results confirm the potential for developing more sustainable and environmentally friendly electrochemical composites and sensors with relatively low cost, ease of production, and large-scale reproducibility.

CRediT authorship contribution statement

Rafaela C. de Freitas: Writing – review & editing, Writing – original draft, Visualization, Validation, Supervision, Methodology, Investigation, Formal analysis, Data curation, Conceptualization. **Jéssica Rocha Camargo:** Writing – review & editing, Writing – original draft, Visualization, Methodology, Investigation, Data curation, Conceptualization. **Laís Canniatti Brazaca:** Writing – review & editing, Visualization, Validation, Methodology, Conceptualization. **Lucio Angnes:** Writing – review & editing, Validation, Methodology, Formal analysis, Conceptualization. **Orlando Fatibello-Filho:** Writing – review & editing, Visualization, Methodology, Investigation, Conceptualization. **Bruno C. Janegitz:** Writing – review & editing, Writing – original draft, Visualization, Validation, Supervision, Resources, Methodology, Investigation, Funding acquisition, Data curation, Conceptualization.

Declaration of competing interest

The authors declare that they have no known competing financial interests or personal relationships that could have appeared to influence the work reported in this paper.

Acknowledgment

The authors thank the financial support provided by Fundação de Amparo à Pesquisa do Estado de São Paulo (2023/06793–4, 2023/10141-2 and 2024/04116–8), Coordenação de Aperfeiçoamento de Pessoal de Nível Superior (CAPES, 88887.504861/2020–00 and 001), Conselho Nacional de Desenvolvimento Científico e Tecnológico (CNPq 381660/2024–9, 401977/2023–4, 401681/2023–8, 301796/2022–0 and 308996-2023-2), Financiadora de Estudos e Projetos (FINEP,

MARTMA, #01.22.0179.00) and, INCT Nanoagro (405924/2022-4); INCT-Bioanalítica (14/50867-3) and INCT-Nanovida (406079/2022-6).

Appendix A. Supplementary data

Supplementary data to this article can be found online at <https://doi.org/10.1016/j.talanta.2025.128875>.

Data availability

Data will be made available on request.

References

- [1] R.A.A. Muñoz, Sustainable and economical platforms for electrochemical (bio) chemical sensing based on micro- and nanotechnologies, *Microchim. Acta* 190 (12) (2023) 486, <https://doi.org/10.1007/s00604-023-06058-6>.
- [2] G. Moro, F. Bottari, J. Van Loon, E. Du Bois, K. De Wael, L.M. Moretto, Disposable electrodes from waste materials and renewable sources for (bio) electroanalytical applications, *Biosens. Bioelectron.* 146 (2019) 111758, <https://doi.org/10.1016/j.bios.2019.111758>.
- [3] A.G.-M. Ferrari, S.J. Rowley-Neale, C.E. Banks, Screen-printed electrodes: transitioning the laboratory in-to-the field, *Talanta Open* 3 (2021) 100032, <https://doi.org/10.1016/j.talo.2021.100032>.
- [4] R.M. Silva, A.D. da Silva, J.R. Camargo, B.S. de Castro, L.M. Meireles, P.S. Silva, B. C. Janegitz, T.A. Silva, Carbon nanomaterials-based screen-printed electrodes for sensing applications, *Biosensors* 13 (4) (2023) 453, <https://doi.org/10.3390/bios13040453>.
- [5] A. Hayat, J.L. Marty, Disposable screen printed electrochemical sensors: tools for environmental monitoring, *Sensors* 14 (6) (2014) 10432–10453, <https://doi.org/10.3390/s140610432>.
- [6] J.R. Camargo, L.O. Orzari, D.A.G. Araujo, P.R. de Oliveira, C. Kalinke, D.P. Rocha, A.L. dos Santos, R.M. Takeuchi, R.A.A. Munoz, J.A. Bonacin, Development of conductive inks for electrochemical sensors and biosensors, *Microchem. J.* 164 (2021) 105998, <https://doi.org/10.1016/j.microc.2021.105998>.
- [7] S.N. Hapuarachchi, K.C. Wasalathilake, J.Y. Nerkar, E. Jaatinen, A.P. O'Mullane, C. Yan, Mechanically robust tapioca starch composite binder with improved ionic conductivity for sustainable lithium-ion batteries, *ACS Sustain. Chem. Eng.* 8 (26) (2020) 9857–9865, <https://doi.org/10.1021/acsschemeng.0c02843>.
- [8] N. Javadian, A. Mohammadi Nafchi, M. Bolandi, The effects of dual modification on functional, microstructural, and thermal properties of tapioca starch, *Food Sci. Nutr.* 9 (10) (2021) 5467–5476, <https://doi.org/10.1002/fsn3.2506>.
- [9] G.C. Mauruto de Oliveira, E.P. de Palma, M.H. Kunita, R. Antigo Medeiros, R. de Matos, K.R. Francisco, B.C. Janegitz, Tapioca biofilm containing Nitrogen-doped titanium dioxide nanoparticles for electrochemical detection of 17- β estradiol, *Electroanalysis* 29 (11) (2017) 2638–2645, <https://doi.org/10.1002/elan.201700392>.
- [10] F.C. Vicentini, L.R.G. Silva, J.S. Stefano, A.R.F. Lima, J. Prakash, J.A. Bonacin, B. C. Janegitz, Starch-based electrochemical sensors and biosensors: a review, *Biomed. Mater. Devices* 1 (1) (2023) 319–338, <https://doi.org/10.1007/s44174-022-00012-5>.
- [11] A. Singh, A. Sharma, A. Ahmed, A.K. Sundramoorthy, H. Furukawa, S. Arya, A. Khosla, Recent advances in electrochemical biosensors: applications, challenges, and future scope, *Biosensors* 11 (9) (2021) 336, <https://doi.org/10.3390/bios11090336>.
- [12] K.U.K. Nampoothiri, V. Krishnakumar, P.K. Thampan, M.A. Nair, *The Coconut Palm (Cocos nucifera L.)—Research and Development Perspectives*, Springer, 2019.
- [13] L.J. Pham, Coconut (cocos nucifera). *Industrial Oil Crops*, Elsevier, 2016, pp. 231–242.
- [14] A.L. Sanford, S.W. Morton, K.L. Whitehouse, H.M. Oara, L.Z. Lugo-Morales, J. G. Roberts, L.A. Somers, Voltammetric detection of hydrogen peroxide at carbon fiber microelectrodes, *Anal. Chem.* 82 (12) (2010) 5205–5210, <https://doi.org/10.1021/ac100536s>.
- [15] B. Wang, X. Wen, P.Y. Chiou, N.T. Maidment, Pt nanoparticle-modified carbon fiber microelectrode for selective electrochemical sensing of hydrogen peroxide, *Electroanalysis* 31 (9) (2019) 1641–1645, <https://doi.org/10.1002/elan.201900362>.
- [16] D. Plausinaitis, L. Sinkevicius, U. Samukaite-Bubniene, V. Ratautaite, A. Ramanavicius, Evaluation of electrochemical quartz crystal microbalance based sensor modified by uric acid-imprinted polypyrrole, *Talanta* 220 (2020) 121414, <https://doi.org/10.1016/j.talanta.2020.121414>.
- [17] G. Ndrepepa, Uric acid and cardiovascular disease, *Clin. Chim. Acta* 484 (2018) 150–163, <https://doi.org/10.1016/j.cca.2018.05.046>.
- [18] G. Turkkkan, S.Z. Bas, K. Atacan, M. Ozmen, An electrochemical sensor based on a Co 3 O 4-ERGO nanocomposite modified screen-printed electrode for detection of uric acid in artificial saliva, *Anal. Methods* 14 (1) (2022) 67–75, <https://doi.org/10.1039/D1AY01744F>.
- [19] L. Xing, W. Zhang, L. Fu, J.M. Lorenzo, Y. Hao, Fabrication and application of electrochemical sensor for analyzing hydrogen peroxide in food system and biological samples, *Food Chem.* 385 (2022) 132555, <https://doi.org/10.1016/j.foodchem.2022.132555>.
- [20] T. Ahmad, A. Iqbal, S.A. Halim, J. Uddin, A. Khan, S. El Deeb, A. Al-Harrasi, Recent advances in electrochemical sensing of hydrogen peroxide (H2O2) released from cancer cells, *Nanomaterials* 12 (9) (2022) 1475, <https://doi.org/10.3390/nano12091475>.
- [21] M. Bilgi Kamac, E. Kiyamaz Onat, M. Yilmaz, A novel non-enzymatic amperometric H2O2 sensor based on screen-printed electrode modified with reduced graphene oxide, polynitralred and gold nanoparticles, *Int. J. Environ. Anal. Chem.* 100 (4) (2020) 408–418, <https://doi.org/10.1080/03067319.2019.1700975>.
- [22] A.M. Campos, P.A. Raymundo-Pereira, C.D. Mendonca, M.L. Calegari, S. A. Machado, O.N. Oliveira Jr., Size control of carbon spherical shells for sensitive detection of paracetamol in sweat, saliva, and urine, *ACS Appl. Nano Mater.* 1 (2) (2018) 654–661, <https://doi.org/10.1021/acsanm.7b00139>.
- [23] J.V.B. Kozan, R.P.d. Silva, S.H.P. Serrano, A.W.O. Lima, L. Angnes, Biosensing hydrogen peroxide utilizing carbon paste electrodes containing peroxidases naturally immobilized on coconut (cocos nucifera L.) fibers, *Anal. Chim. Acta* 591 (2) (2007) 200–207, <https://doi.org/10.1016/j.aca.2007.03.058>.
- [24] H. Li, M.A. Huneault, Comparison of sorbitol and glycerol as plasticizers for thermoplastic starch in TPS/PLA blends, *J. Appl. Polym. Sci.* 119 (4) (2011) 2439–2448, <https://doi.org/10.1002/app.32956>.
- [25] J.R. Camargo, I.A. Andreotti, C. Kalinke, J.M. Henrique, J.A. Bonacin, B. C. Janegitz, Waterproof paper as a new substrate to construct a disposable sensor for the electrochemical determination of paracetamol and melatonin, *Talanta* (2019) 120458–120466, <https://doi.org/10.1016/j.talanta.2019.120458>.
- [26] L.O. Orzari, L.R.G.e. Silva, R.C. de Freitas, L.C. Brazaca, B.C. Janegitz, Lab-made disposable screen-printed electrochemical sensors and immunosensors modified with Pd nanoparticles for Parkinson's disease diagnostics, *Microchim. Acta* 191 (1) (2024) 76–91, <https://doi.org/10.1007/s00604-023-06158-3>.
- [27] L.A. Pradela-Filho, I.A. Andreotti, J.H. Carvalho, D.A. Araujo, L.O. Orzari, A. Gatti, R.M. Takeuchi, A.L. Santos, B.C. Janegitz, Glass varnish-based carbon conductive ink: a new way to produce disposable electrochemical sensors, *J. Sensors Actuators B: Chem* 305 (2020) 127433, <https://doi.org/10.1016/j.snb.2019.127433>.
- [28] A. Neumann, L.O.v. Orzari, J.A. Bonacin, B.C. Janegitz, Properties evaluation of different graphite brands through the development of electrochemical sensors for phenolic compounds detection, *ACS Omega* (2025), <https://doi.org/10.1021/acsomega.4c10281>.
- [29] J.H.S. Carvalho, J.L. Gogola, M.F. Bergamini, L.H. Marcolino-Junior, B.C. Janegitz, Disposable and low-cost lab-made screen-printed electrodes for voltammetric determination of L-dopa, *Sens. Actuators Rep.* 3 (2021) 100056, <https://doi.org/10.1016/j.snr.2021.100056>.
- [30] J.R. Macdonald, W.B. Johnson, I.D. Raistrick, D.R. Franceschetti, N. Wagner, M.C. H. McKubre, D.D. Macdonald, B. Sayers, N. Bonanos, B.C.H. Steele, *Impedance Spectroscopy: Theory, Experiment, and Applications*, John Wiley, 2018. & Sons.
- [31] A.C. Lazanas, M.I. Prodromidis, Electrochemical impedance spectroscopy— a tutorial, *ACS Meas. Sci. Au.* 3 (3) (2023) 162–193, <https://doi.org/10.1021/acsmesureciau.2c00070>.
- [32] L.M. Gassa, J.R. Vilche, M. Ebert, K. Jüttner, W.J. Lorenz, Electrochemical impedance spectroscopy on porous electrodes, *J. Appl. Electrochem.* 20 (4) (1990) 677–685, <https://doi.org/10.1007/BF01008882>.
- [33] D.L. Pavia, G.M. Lampman, G.S. Kriz, J.R. Vyvyan, *Infrared Spectroscopy, Introduction to Spectroscopy*, Brooks/Cole, Cengage Learning, United States of America, 2009, p. 752.
- [34] P. Deeyai, M. Suphantharika, R. Wongsagonsup, S. Dangtip, Characterization of modified tapioca starch in atmospheric argon plasma under diverse humidity by FTIR spectroscopy, *Chin. Phys. Lett.* 30 (1) (2013) 018103, <https://doi.org/10.1088/0256-307X/30/1/018103>.
- [35] S.-M. Lee, S.-H. Lee, J.-S. Roh, Analysis of activation process of carbon black based on structural parameters obtained by XRD analysis, *Crystals* 11 (2) (2021) 153–164, <https://doi.org/10.3390/cryst11020153>.
- [36] A. Nezzal, L. Aerts, M. Verspaille, G. Henderickx, A. Redl, Polymorphism of sorbitol, *J. Cryst. Growth* 311 (15) (2009) 3863–3870, <https://doi.org/10.1016/j.jcrysgro.2009.06.003>.
- [37] R.A. Gómez-López, C.E. Montilla-Buitrago, H.S. Villada-Castillo, A. Sáenz-Galindo, F. Avalos-Belmontes, L. Serna-Cock, Co-plasticization of starch with glycerol and isosorbide: effect on retrogradation in thermo-plastic cassava starch films, *Polymers* 15 (9) (2023) 2104, <https://doi.org/10.3390/polym15092104>.
- [38] L.O. Orzari, R.C. de Freitas, I.A. de Araujo Andreotti, A. Gatti, B.C. Janegitz, A novel disposable self-adhesive inked paper device for electrochemical sensing of dopamine and serotonin neurotransmitters and biosensing of glucose, *Biosens. Bioelectron.* 138 (2019) 111310, <https://doi.org/10.1016/j.bios.2019.05.015>.
- [39] I. Ali, M. Ahmad, S. Ridha, C.C. Iferobia, N. Lashari, Dual modification approach for tapioca starch using gamma irradiation and carboxymethylation, *Hybrid Adv.* 3 (2023) 100071, <https://doi.org/10.1016/j.hybadv.2023.100071>.
- [40] A. Darmawan, S.D. Miftiyati, C. Azmiyawati, Synthesis of carbon membranes using sorbitol as a carbon source for desalination applications, *J. Mater. Eng. Perform.* (2023) 1–11, <https://doi.org/10.1007/s11665-023-08653-3>.
- [41] X. Ma, C. Qiao, J. Zhang, J. Xu, Effect of sorbitol content on microstructure and thermal properties of chitosan films, *Int. J. Biol. Macromol.* 119 (2018) 1294–1297, <https://doi.org/10.1016/j.jbiomac.2018.08.060>.
- [42] F. Farivar, P.L. Yap, R.U. Karunakaran, D. Losic, Thermogravimetric analysis (TGA) of graphene materials: effect of particle size of graphene, graphene oxide and graphite on thermal parameters, *C — J. Carbon Res.* 7 (2) (2021) 41, <https://doi.org/10.3390/c7020041>.
- [43] P. Sakthivel, K. Ramachandran, K. Maheshvaran, T.S. Senthil, P. Manivel, Simultaneous electrochemical detection of ascorbic acid, dopamine and uric acid using Au decorated carbon nanofibers modified screen printed electrode, *Carbon Lett.* (2024) 1–17, <https://doi.org/10.1007/s42823-024-00759-5>.

- [44] K. Aoki, M. Ishida, K. Tokuda, K. Hasebe, Electrode kinetics of the oxidation of hydrogen peroxide at pretreated glassy carbon and carbon fiber electrodes, *J. Electroanal. Chem. Interfacial Electrochem.* 251 (1) (1988) 63–71, [https://doi.org/10.1016/0022-0728\(88\)80385-1](https://doi.org/10.1016/0022-0728(88)80385-1).
- [45] L.R. Wilson, S. Panda, A.C. Schmidt, L.A. Sombers, Selective and mechanically robust sensors for electrochemical measurements of real-time hydrogen peroxide dynamics in vivo, *Anal. Chem.* 90 (1) (2018) 888–895, <https://doi.org/10.1021/acs.analchem.7b03770>.
- [46] F. Seven, T. Gölce, Nanoporous carbon-fiber microelectrodes for sensitive detection of H₂O₂ and dopamine, *J. Electroanal. Chem.* 864 (2020) 114104, <https://doi.org/10.1016/j.jelechem.2020.114104>.
- [47] W. Warsakoon, Preliminary study on heavy metals in coconut and coconut products, *CORD* 26 (1) (2010) 7, <https://doi.org/10.37833/cord.v26i1.132>, 7.
- [48] J.W.H. Yong, L. Ge, Y.F. Ng, S.N. Tan, The chemical composition and biological properties of coconut (*Cocos nucifera* L.) water, *Molecules* 14 (12) (2009) 5144–5164, <https://doi.org/10.3390/molecules14125144>.
- [49] S. Chen, R. Yuan, Y. Chai, F. Hu, Electrochemical sensing of hydrogen peroxide using metal nanoparticles: a review, *Microchim. Acta* 180 (2013) 15–32, <https://doi.org/10.1007/s00604-012-0904-4>.
- [50] A. Liu, H. Geng, C. Xu, H. Qiu, A three-dimensional hierarchical nanoporous PdCu alloy for enhanced electrocatalysis and biosensing, *Anal. Chim. Acta* 703 (2) (2011) 172–178, <https://doi.org/10.1016/j.aca.2011.07.039>.
- [51] T.-J. Lin, K.-T. Yen, C.-F. Chen, S.-T. Yan, K.-W. Su, Y.-L. Chiang, Label-free uric acid estimation of spot urine using portable device based on UV spectrophotometry, *Sensors* 22 (8) (2022) 3009, <https://doi.org/10.3390/s22083009>.
- [52] P. Kanyong, S. Rawlinson, J. Davis, A voltammetric sensor based on chemically reduced graphene oxide-modified screen-printed carbon electrode for the simultaneous analysis of uric acid, ascorbic acid and dopamine, *Chemosensors* 4 (4) (2016) 25, <https://doi.org/10.3390/chemosensors4040025>.
- [53] R. Jirakunakorn, S. Khumngern, J. Choosang, P. Thavarungkul, P. Kanatharana, A. Numnuam, Uric acid enzyme biosensor based on a screen-printed electrode coated with Prussian blue and modified with chitosan-graphene composite cryogel, *Microchem. J.* 154 (2020) 104624, <https://doi.org/10.1016/j.microc.2020.104624>.
- [54] F.S. da Cruz, F. de Souza Paula, D.L. Franco, W.T.P. dos Santos, L.F. Ferreira, Electrochemical detection of uric acid using graphite screen-printed electrodes modified with Prussian blue/poly (4-aminosalicylic acid)/uricase, *J. Electroanal. Chem.* 806 (2017) 172–179, <https://doi.org/10.1016/j.jelechem.2017.10.070>.
- [55] P. Fanjul-Bolado, D.H. Santos, V.M. Montoya, A. Costa-García, Uric acid determination by adsorptive stripping voltammetry on multiwall carbon nanotubes based screen-printed electrodes, *Electroanalysis* 27 (5) (2015) 1276–1281, <https://doi.org/10.1002/elan.201400690>.
- [56] C. Maksuk, C. Tinala, W. Somboot, J. Jakmunee, F. Marken, T. Kanyanee, Rapid determination of hydrogen peroxide in milk with non-enzymatic amperometric sensor based on porous gold modified screen-printed electrode in online dialysis System, *Electroanalysis* 35 (2) (2023) e202100691, <https://doi.org/10.1002/elan.202100691>.
- [57] M. Devaraj, S. Rajendran, J.N. Jebaranjitham, D. Ranjithkumar, M. Sathiyaraj, J. Manokaran, E. Sundaravadeivel, J. Santhanalakshmi, L.C. Ponce, Horseradish peroxidase-immobilized graphene oxide-chitosan gold nanocomposites as highly sensitive electrochemical biosensor for detection of hydrogen peroxide, *J. Electrochem. Soc.* 167 (14) (2020) 147517, <https://doi.org/10.1149/1945-7111/abc35e>.
- [58] X. Bian, X. Lu, E. Jin, L. Kong, W. Zhang, C. Wang, Fabrication of Pt/polypyrrole hybrid hollow microspheres and their application in electrochemical biosensing towards hydrogen peroxide, *Talanta* 81 (3) (2010) 813–818, <https://doi.org/10.1016/j.talanta.2010.01.020>.
- [59] M. Guler, V. Turkoglu, A. Bulut, M. Zahmakiran, Electrochemical sensing of hydrogen peroxide using Pd@ Ag bimetallic nanoparticles decorated functionalized reduced graphene oxide, *Electrochim. Acta* 263 (2018) 118–126, <https://doi.org/10.1016/j.electacta.2018.01.048>.
- [60] F. Pena-Pereira, W. Wojnowski, M. Tobiszewski, AGREE—Analytical GREENness metric approach and software, *Anal. Chem.* 92 (14) (2020) 10076–10082, <https://doi.org/10.1021/acs.analchem.0c01887>.
- [61] S.S. Soliman, G.A. Sedik, M.R. Elghobashy, H.E. Zaazaa, A.S. Saad, Greenness assessment profile of a QbD screen-printed sensor for real-time monitoring of sodium valproate, *Microchem. J.* 182 (2022) 107859, <https://doi.org/10.1016/j.microc.2022.107859>.